(Received 3 November 2023, Accepted 23 January 2024, Scheduled 7 February 2024)

A Method of Reducing Coupling between PIFA Antennas Using Cross Slot Defected Ground Structure

Hao Zhang[1], Yafei Wang[1, 2, *], and Xuehua Li[1, 2]

[1]*Key Laboratory of Information and Communication Systems, Ministry of Information Industry Beijing Information Science and Technology University, Beijing 100101, China*
[2]*Key Laboratory of Modern Measurement & Control Technology , Ministry of Education Beijing Information Science and Technology University, Beijing 100101, China*

ABSTRACT: To reduce the coupling between closely packed antenna elements in multiple-input multiple-output (MIMO) systems, a method is proposed to reduce the coupling between planar inverted F-shaped antennas (PIFAs) by using cross slot defected ground structure (CSDGS). This structure includes four intersecting slits etched into the ground plane. The resonant frequency of the PIFA is within the bandgap of the CSDGS, effectively suppressing surface waves and reducing the coupling between antennas. Through simulation, it is demonstrated that the proposed structure achieves more than 35 dB isolation between two antenna elements. To validate the effectiveness of the method, the circuit of the simulated structure is processed and measured using a vector network analyzer. The measured results align closely with the simulated ones, confirming the viability of the proposed method. The parameter study and correlation coefficient of CSDGS are also analyzed.

1. INTRODUCTION

MIMO technology has gained significant attention in the wireless communication field due to its advantages of high speed, large capacity, and robust transmission reliability [1]. It involves the use of multiple antennas in wireless transmitters and receivers to achieve synchronous transmission, thereby increasing the transmission rate and system capacity. By dividing and transmitting the signals, MIMO systems reduce the power of individual signals and extend the transmission distance. This approach effectively improves the frequency spectrum utilization efficiency and enhances the channel capacity of the antenna system [2]. Consequently, the development of MIMO antennas has become a crucial area of research and innovation.

As mobile terminal equipment continues to shrink in size, antenna miniaturization becomes more critical. However, a key challenge arises when the spacing between array elements becomes too small, resulting in strong coupling that significantly impacts the antenna's radiation characteristics. Coupling refers to the interaction between input and output of circuit components, leading to the transfer of energy between them.

Mutual coupling between antenna elements can be classified into two types. The first type is coupling originating from the antenna ground or surface waves. In this case, the signal, in the form of current or surface waves, propagates from the feed port to other ports, causing interference. The second type is radiative coupling from the surrounding transmission space. Not all electromagnetic waves emitted by the feed antenna reach the target antenna; some are received by adjacent antennas, resulting in coupling interference between the two elements.

In the pursuit of antenna miniaturization, wideband operation, and multi-element systems, enhancing antenna isolation through decoupling techniques has become a prominent area of research. Numerous experts and scholars have dedicated their efforts to mitigate the coupling between closely spaced antenna elements. Currently, common approaches include the utilization of electromagnetic band-gap (EBG) structures, neutralization lines, and defected ground structures [3] (DGS).

The EBG structure decoupling method involves the integration of multiple mushroom-shaped metal structures between closely spaced antenna elements. This technique effectively suppresses surface waves within the targeted frequency band, leading to improved isolation between antennas. By incorporating the EBG structure between antenna elements, mutual coupling can be significantly reduced.

A novel EBG structure is proposed to achieve high isolation between MIMO antennas [4]. The study compares the performances of antennas with and without the EBG structure, specifically focusing on the 5G frequency band. The results demonstrate that the MIMO antenna with an EBG structure exhibits an average isolation improvement of 13.9 dB compared to the antenna without it.

Another effective technique for suppressing mutual coupling between antennas is the addition of a neutralization line. This method involves connecting the antenna elements through one or more microstrip lines on the antenna radiation surface, creating an artificial coupling path. By adding a neutralization line, two current paths are established for the non-excited unit: one through the neutralization line and the other through the floor and space coupling. These two paths carry currents with equal amplitude but opposite directions, resulting in cancellation and reducing mutual coupling within the antenna array.

* Corresponding author: Yafei Wang (wangyafei@bistu.edu.cn).

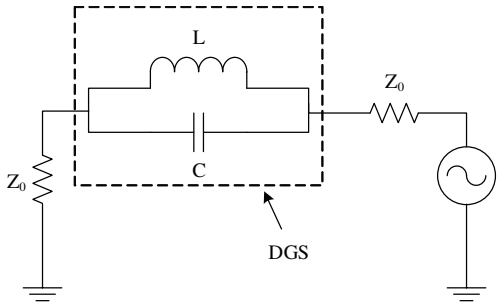

FIGURE 1. The equivalent circuit of DGS.

To address the mutual coupling challenge in small ultra-wideband (UWB) MIMO antennas, a wideband neutralization line is proposed [5]. This decoupling technique enables the design of a MIMO antenna that covers the 3.1 GHz to 5 GHz frequency band, providing isolation levels higher than 22 dB.

While the aforementioned methods effectively reduce the coupling between antenna elements, they do possess certain limitations. The EBG structure is hindered by its large size, which makes it challenging to achieve circuit and antenna miniaturization. Additionally, these structures present difficulties in terms of processing and packaging. Similarly, the neutralization line decoupling method encounters integration challenges. Most existing neutralization lines are designed for binary antenna arrays. However, as the number of antennas increases, multiple coupling paths arise between adjacent antenna elements, resulting in a more complex coupling field. This complexity poses complications in the design of neutralization lines.

DGS is another popular method employed to suppress coupling between antennas. It entails the creation of a periodic or aperiodic structure etched on the metal floor of the microwave transmission line. This structure serves to elongate the path of surface currents on the floor, thereby reducing mutual coupling between antenna elements and enhancing isolation between antenna ports. The DGS decoupling method boasts numerous advantages, including a simple structure, compact size, easy integration, convenient simulation, and practical processing. Moreover, it is compatible with various antenna forms, and its decoupling effect remains consistent regardless of the antenna's specific design.

In Fig. 1, the DGS is depicted as an equivalent circuit comprising capacitors and inductors. For instance, considering a dumbbell-shaped DGS, the inductance of the equivalent circuit is influenced by the size of the DGS head, while the capacitance is affected by the size of the DGS slit. When the frequency of the antenna unit aligns with the resonant frequency of the DGS, the DGS acts to suppress the surface wave of the antenna unit, thereby reducing the coupling.

A novel slot-array DGS is proposed for decoupling microstrip antenna arrays [7]. This approach involves etching slot-array DGS elements around each antenna element on the ground plane, parallel to the radiating edge of each element. Both simulated and measured results demonstrate a significant reduction in mutual coupling, reaching approximately 40 dB across the entire operating band.

Another study by Ouyang et al. proposes a simple and compact decoupling structure achieved by etching a rectangular DGS on the floor between arrays [8]. Simulation results indicate a coupling reduction about 40 dB, with the operating band centered at 5.8 GHz.

A structure consisting of slit patterns etched into a single ground plane is proposed [9]. The results highlight the attainment of isolation levels exceeding 20 dB.

Additionally, a straightforward DGS approach for reducing mutual coupling between closely spaced antenna elements is proposed [10]. By placing two PIFA elements in parallel, isolation levels of more than 40 dB can be achieved.

This paper aims to tackle the design challenges associated with DGS, including the low operating frequency observed in the designed antenna [7–9] and the considerable deviation between the decoupling effects obtained from actual testing and simulation results [10]. To address these concerns, a new structure is proposed, which involves the implementation of CSDGS etched on the ground plane between the PIFA antenna elements. This novel structure effectively mitigates coupling and substantially improves the isolation. The design structure of this paper is novel, which has not been proposed in the previous article. According to the different antenna working band and antenna size, the size can be modified simply on the basis of the designed DGS to achieve coupling reduction. The principle of DGS is also analyzed in this paper.

2. ANTENNA DESIGN

Most mobile phone antennas currently adopt the PIFA design scheme, primarily due to its space-saving advantages. The basic structure of a PIFA antenna comprises a planar radiating element serving as the primary antenna, a ground plane acting as the reflecting surface, and two closely spaced pins on the radiating body for grounding and feeding. By positioning the antenna above and parallel to the PCB, it only occupies the space occupied by the pins. This allows for component installation beneath the antenna, with the PCB being utilized on both sides.

The PIFA's fundamental structure consists of four main components: ground plane, radiating unit, short-circuit metal sheet, and coaxial line. The ground plane serves as a reflecting surface, while the radiating unit comprises a metal sheet parallel to the ground plane. The short-circuit metal sheet connects the radiating unit and ground plane, and the coaxial line facilitates signal transmission.

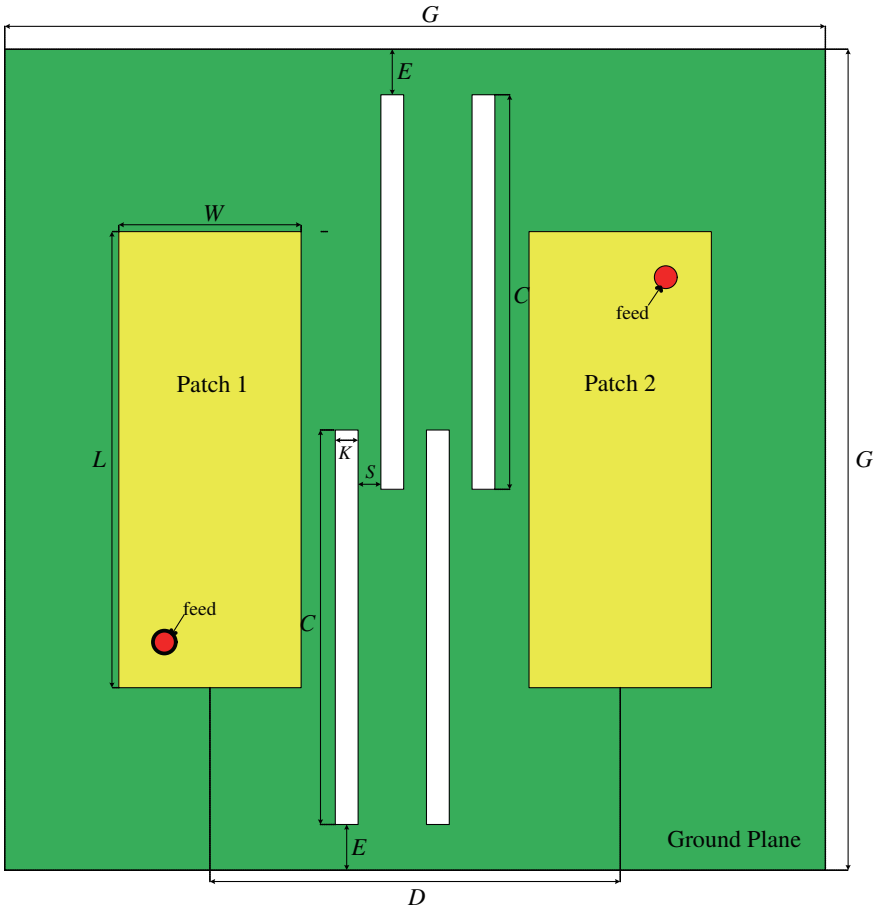

FIGURE 2. PIFA antenna loaded with CSDGS (top view).

To meet the miniaturization requirements of mobile communication terminal equipment, the spacing between PIFA antenna elements is often reduced. However, excessively small spacing between elements can lead to coupling effects, significantly impacting the antenna's radiation characteristics. In this paper, a proposed solution is the implementation of a CSDGS to mitigate coupling between PIFAs. The PIFA loaded with CSDGS is shown in Fig. 2.

In the figure, the size of the PIFA is: $L*W = 20\,\text{mm}*8\,\text{mm}$; the distance between the two antenna elements is: $D = 18\,\text{mm}$; the height of distance from the ground plane to the patch is: $h = 5\,\text{mm}$; the dimensions of the ground plane are: $G*G = 36\,\text{mm}*36\,\text{mm}$; the size of slits is: $C*K = 17.3\,\text{mm}*0.9\,\text{mm}$; the distance between each slit is: $S = 1\,\text{mm}$; the distance between the slit and the floor boundary is $E = 2\,\text{mm}$. In order to reduce the spacing between the elements, the PIFA is excited from different directions.

3. EXPERIMENTAL AND MEASUREMENT RESULT

In this section, the effectiveness of the CSDGS structure in suppressing coupling between PIFAs is examined through simulations conducted using HFSS software. The simulation frequency is set in the range of 6 GHz to 9 GHz, and the obtained results encompass various parameters, including S parameters, surface current distribution, and 3D far-field radiation pattern. These simulations aim to verify the impact of the proposed PIFA with CSDGS structure on coupling suppression.

3.1. S Parameter

The performance of a PIFA can be evaluated using two key parameters: S_{11} and S_{21}. S_{11} represents the reflection coefficient of the antenna port, indicating the amount of energy reflected from the antenna port. It is calculated as the ratio between the power of the signal reflected back to the port and the power of the signal emitted by the antenna port. S_{21} measures the coupling coefficient from the first port to the second port. It quantifies the ratio of the signal power at the second port to the signal power at the first port. A smaller value of S_{21} indicates a lower coupling between the two ports.

The resonant frequency of an antenna refers to the frequency range within which the antenna meets the operational requirements for effective signal reception and transmission. In the case of a PIFA, the resonant frequency is typically defined as the frequency range where the antenna's return loss, represented by S_{11}, is below $-10\,\text{dB}$. The center frequency of the antenna is defined as the frequency corresponding to the lowest S_{11} within this resonant frequency range. At the center frequency, the antenna is optimized to deliver its best performance, achieving the

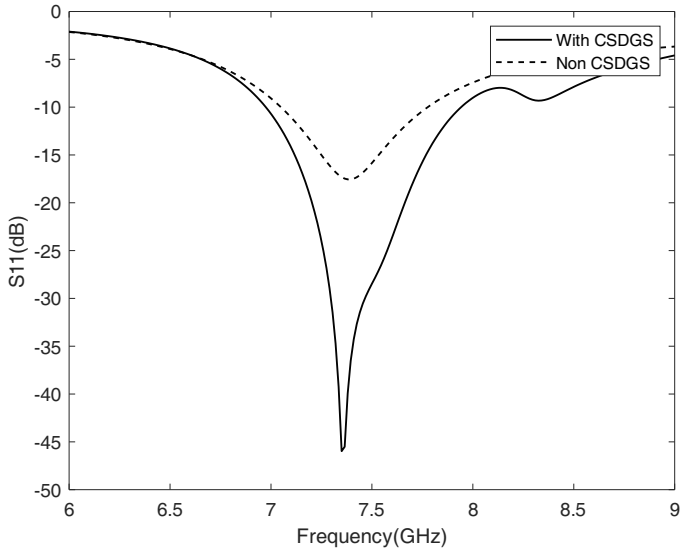

FIGURE 3. S_{11} simulation results with and without CSDGS.

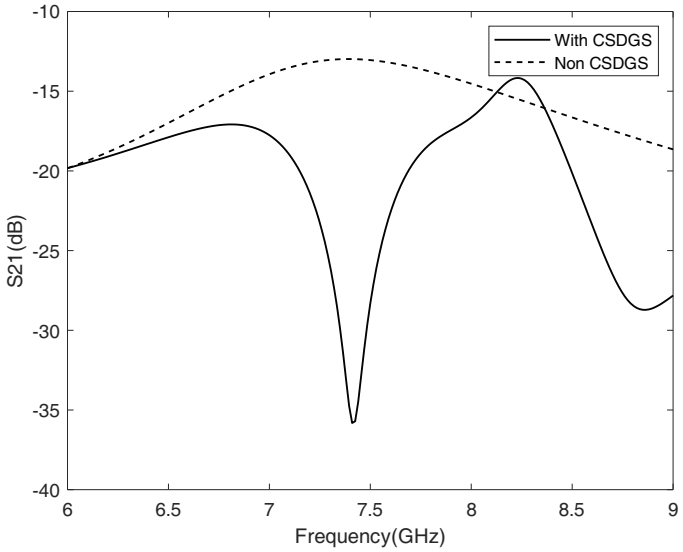

FIGURE 4. S_{21} simulation results with and without CSDGS.

highest efficiency in both receiving and transmitting signals. It is at this center frequency that the antenna exhibits the greatest response and energy conversion efficiency to signals.

The simulation results for S_{11} are presented in Fig. 3. Upon examination, it is evident that the center frequency of the antenna with CSDGS does not undergo significant changes in comparison to the antenna without CSDGS. However, the S_{11} value at the center frequency experiences a decrease of approximately 23 dB when the CSDGS structure is implemented. Moreover, the antenna with CSDGS exhibits a wider bandwidth than the antenna without CSDGS. Specifically, the bandwidth increases from 0.73 GHz to 0.98 GHz.

Figure 4 illustrates the simulation results obtained for S_{21}. The analysis of these results demonstrates that, without the CSDGS structure, the coupling between the antennas at the center frequency is measured at -12.98 dB. However, the addition of the CSDGS structure causes the resonant frequency of the antenna to align with the bandgap of the CSDGS, effectively suppressing surface waves. Consequently, the value of S_{21} at the center frequency decreases to -35.53 dB, which represents a 22.55 dB reduction compared to the antenna without the CSDGS structure. Furthermore, in the frequency range of 7.0 GHz to 7.7 GHz, the average reduction in coupling between the PIFA antenna elements amounts to 11.55 dB.

3.2. Surface Current Distribution

To enhance our comprehension of the CSDGS mechanism, HFSS software can be utilized to simulate the surface current distribution of the antenna radiation elements, enabling further analysis. Fig. 5 and Fig. 6 illustrate the surface current distributions of the antenna radiation elements with and without the CSDGS structure, respectively. By comparing the results depicted in these two figures, it becomes evident that the current flowing from the left radiation element to the right radiation element in the PIFA antenna undergoes substantial reduction when the CSDGS structure is incorporated. This reduction in current effectively mitigates the mutual coupling between the antennas.

3.3. Far-Field Radiation Pattern

The antenna pattern is a graphical representation that illustrates the relationship between the radiation characteristics of an antenna and the spatial angle. The pattern provides valuable insights into how the antenna radiates or receives signals in different directions.

The directivity coefficient, which can be obtained from the radiation pattern, quantifies the directionality of the antenna. The antenna gain is then calculated as the product of the directivity coefficient and the antenna efficiency. A higher gain indicates a more focused radiation pattern with narrower main and side lobes. Antenna gain serves as a measure of an antenna's ability to transmit and receive signals effectively in a specific direction. This parameter plays a crucial role in selecting base station antennas. Given the same conditions, a higher gain allows the signal to propagate over greater distances.

The 3D far-field radiation patterns of the simulated PIFA with and without CSDGS structure are shown in Fig. 7 and Fig. 8, respectively. As can be seen from the figures, the antenna main polarization axial gain is 6.737 dB and 6.567 dB, respectively, which is basically stable. The results show that the CSDGS has no effect on antenna gain while the isolation between antenna elements is improved.

Figures 9 and 10 show the comparison results of far-field radiation patterns of E plane and H plane with and without CSDGS antenna, respectively. As can be seen from the figure, the forward radiation of the antenna has hardly changed, while the backward radiation of the antenna has increased by about 5 dB at most, which is caused by the addition of CSDGS.

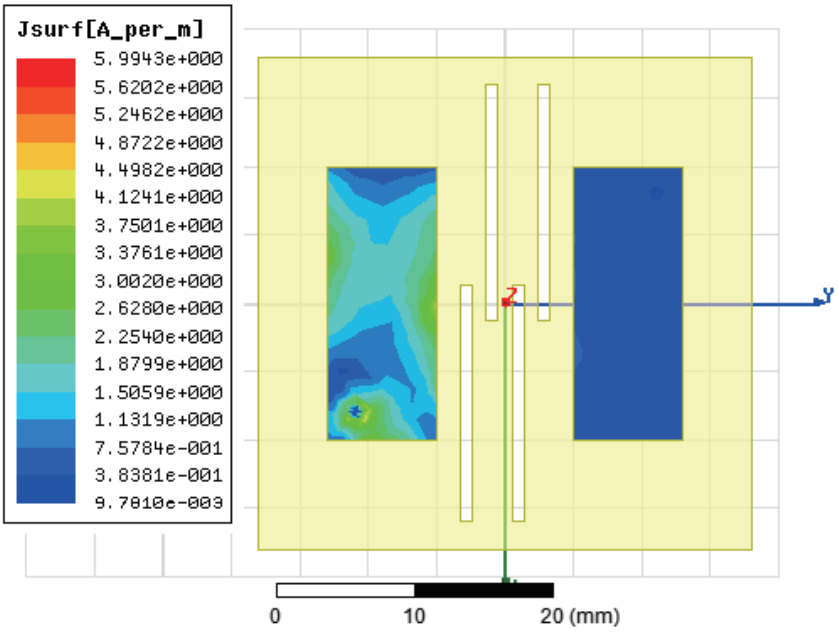

FIGURE 5. Surface current distribution of radiation elements with CSDGS.

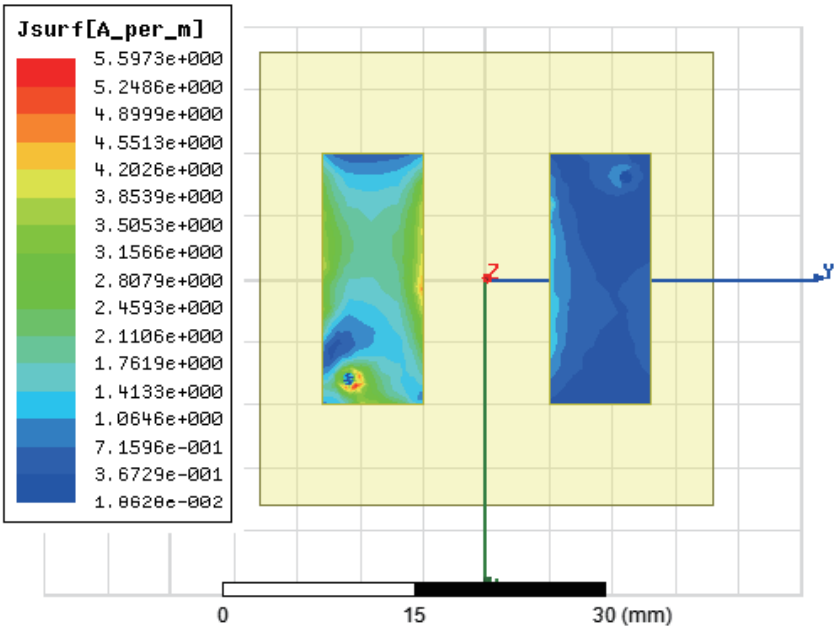

FIGURE 6. Surface current distribution of radiation elements without CSDGS.

3.4. Correlation Coefficient

In a MIMO system, there are many factors affecting the performance of the system, one of which is the spatial correlation of the signal. The spatial correlation of the MIMO antenna refers to the correlation characteristics between the antennas at the transmitting end and the antennas at the receiving end, which is generally expressed by the correlation coefficient. If the correlation coefficient is too large, the channel capacity of MIMO system will be significantly lost. In order to obtain good MIMO performance, one of the necessary conditions is a low correlation between the antennas at the transmitting and receiving ends.

The envelope correlation coefficient (ECC) is defined as the correlation between two signal envelopes, and the calculation formula is shown in formula (1):

$$\rho_e = \frac{E\left\{\left(|x_1|^2 - E\left\{|x_1|^2\right\}\right)\left(|x_2|^2 - E\left\{|x_2|^2\right\}\right)^*\right\}}{\sqrt{E\left\{\left||x_1|^2 - E\left\{|x_1|^2\right\}\right|^2\right\} E\left\{\left||x_2|^2 - E\left\{|x_2|^2\right\}\right|^2\right\}}} \quad (1)$$

x_1 and x_2 represent the two shunt signals, respectively. $E\{\cdot\}$ represents the expected value of the signal. ρ_e is the ECC of antenna.

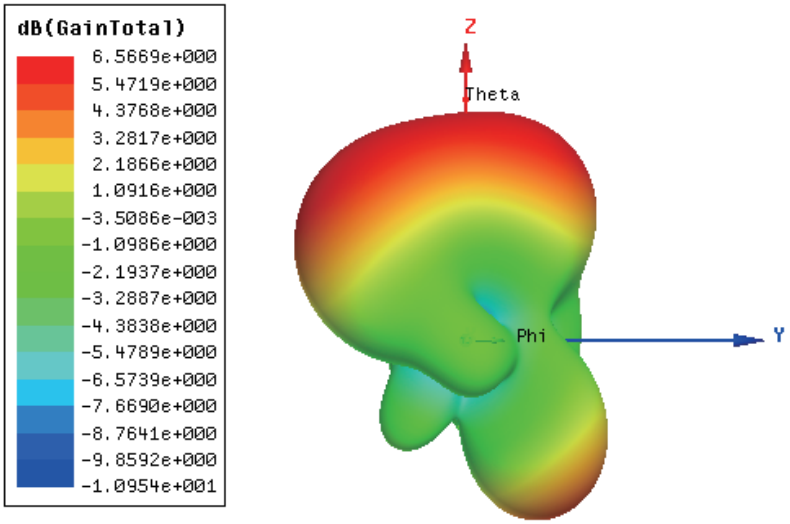

FIGURE 7. 3D far-field radiation pattern of PIFA with CSDGS.

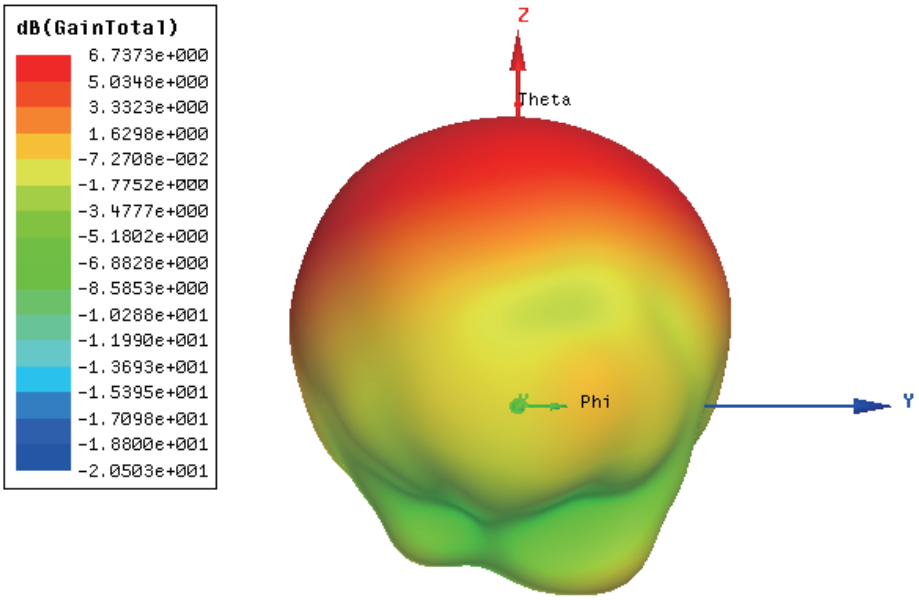

FIGURE 8. 3D far-field radiation pattern of PIFA without CSDGS.

Calculated by HFSS, the correlation coefficients of antennas with and without CSDGS are shown in Fig. 11. The figure shows that the addition of the structure results in a significant reduction in the correlation coefficient between the two antennas. This reduction indicates that the isolation between the antennas has been significantly improved with the CSDGS.

3.5. Parameter Study

It can be seen from the simulation results that CSDGS has a positive effect on reducing coupling. In order to optimize the proposed CSDGS, the parameters of the structure were optimized by HFSS software. Scanning parameters include K, S, C, and E. Three parameters are fixed unchanged, and the fourth parameter is scanned within the effective range. When the fourth parameter changes, the resonant frequency, operating bandwidth, and S_{21} at the resonant frequency corresponding to the antenna are recorded. The summary of experimental data is shown in Table 1.

It can be seen that when K, S, and E are unchanged, C increases from 17.2 mm to 17.4 mm, and S_{21} at the center frequency first decreases and then rises, reaching the best at 17.3 mm. When K, C, and E are unchanged, S increases from 0.9 mm to 1.1 mm, and S_{21} at the center frequency first decreases and then increases, reaching the best at 1.0 mm. When S, C, and E are unchanged, K increases from 0.8 mm to 1.1 mm, and S_{21} at the center frequency first decreases and then increases, reaching the best value at 0.9 mm. When K, S, and C are unchanged, E increases from 1.5 mm to 2.5 mm, and S_{21}

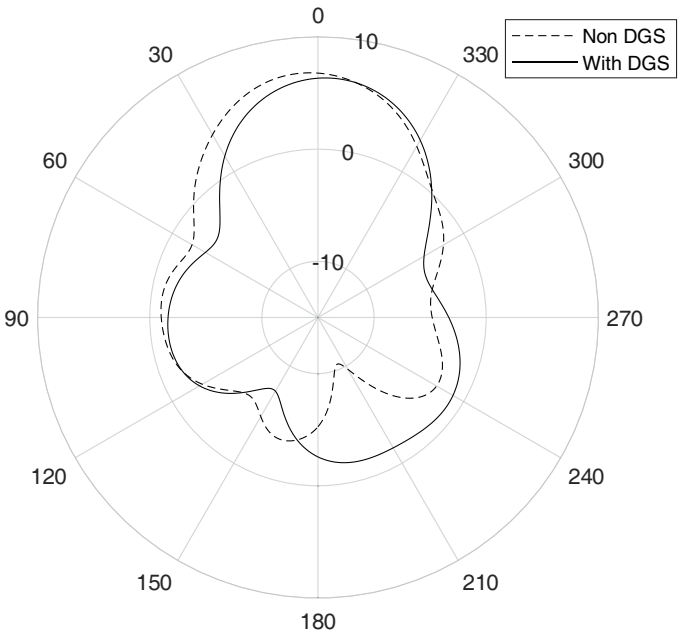

FIGURE 9. Far-field radiation pattern of E plane with and without CSDGS.

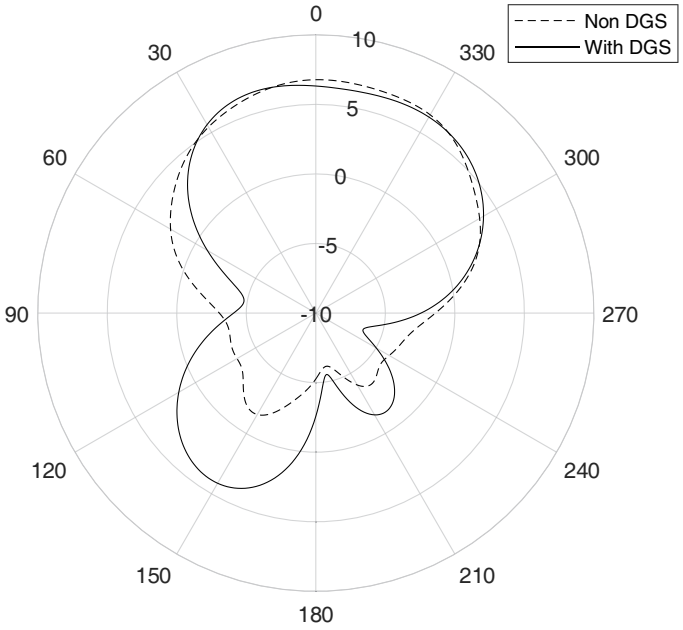

FIGURE 10. Far-field radiation pattern of H plane with and without CSDGS.

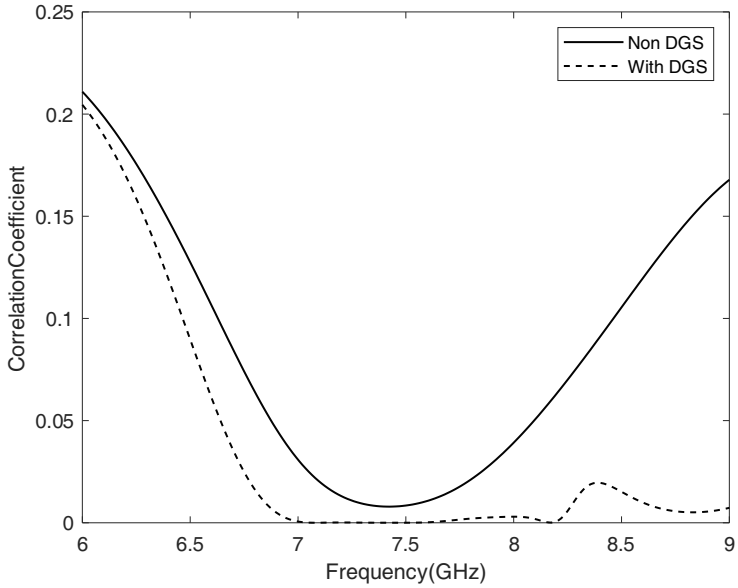

FIGURE 11. Comparison of correlation coefficients with and without CSDGS.

at the center frequency first decreases and then rises, reaching the best at 2.0 mm. So, we can find an optimal K, S, C, E. When $K = 0.9$ mm, $S = 1$ mm, $C = 17.3$ mm, $E = 2$ mm, the S_{21} at the resonant frequency is -35.526 dB, which is smaller than any other case. In this case, the bandwidth of the antenna is 0.931 GHz.

3.6. Performance Comparison

The performance of different structures was investigated in accordance with the references mentioned. The study aimed to explore and evaluate the characteristics and capabilities of these structures. The investigation involved analyzing and comparing various parameters, such as resonant frequency and S_{21} at resonant frequency.

The results are shown in Table 2. As can be seen from the table, CSDGS decoupling effect is better than other structures.

3.7. Measurement

In order to further verify the effect of CSDGS in reducing the coupling, the PIFA with CSDGS was processed and measured by vector network analyzer. The prototype of PIFA with CS-

TABLE 1. PIFA mutual coupling summary table of different parameters.

K	S	C	E	Resonant frequency (GHz)	Operating bandwidth (GHz)	S_{21} at resonant frequency (dB)
1 mm	1 mm	17.2 mm	2 mm	7.341	0.992	−24.412
1 mm	1 mm	17.3 mm	2 mm	7.384	0.966	−34.967
1 mm	1mm	17.4 mm	2 mm	7.484	0.945	−25.197
1 mm	0.9 mm	17.3 mm	2 mm	7.354	0.966	−24.228
1 mm	1 mm	17.3 mm	2 mm	7.384	0.966	−34.967
1 mm	1.1 mm	17.3 mm	2 mm	7.46	0.985	−28.421
0.8 mm	1 mm	17.3 mm	2 mm	7.355	0.948	−20.308
0.9 mm	1 mm	17.3 mm	2 mm	7.394	0.931	−35.526
1 mm	1 mm	17.3 mm	2 mm	7.384	0.966	−34.967
1.1 mm	1 mm	17.3 mm	2 mm	7.362	1.001	−30.395
1 mm	1 mm	17.3 mm	2.5 mm	7.485	0.946	−25.354
1 mm	1 mm	17.3 mm	2 mm	7.384	0.966	−34.967
1 mm	1 mm	17.3 mm	1.5 mm	7.362	1.343	−25.323

TABLE 2. PIFA mutual coupling comparison of different structures.

Structure	Resonant frequency	S_{21} at resonant frequency
CSDGS	7.394 GHz	−35.526 dB
Dumbbell [10]	7.365 GHz	−18.601 dB
SRR [11]	7.750 GHz	−26.760 dB

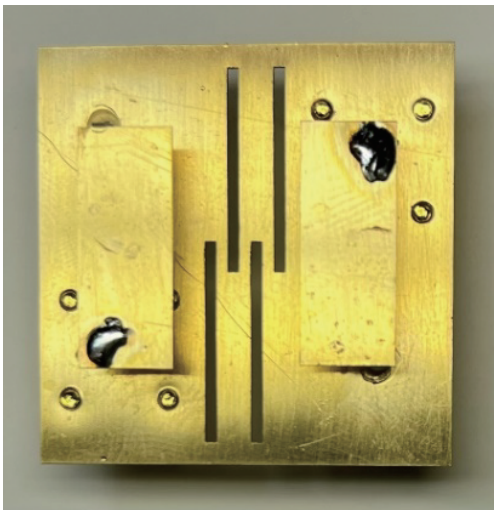

FIGURE 12. The prototype of PIFA with CSDGS.

DGS is shown in Fig. 12. The actual production parameters are consistent with the simulation parameters.

The comparison results of the measured and simulated S_{11} are shown in Fig. 13. It can be seen from the results that the measured antenna bandwidth is 0.96 GHz, which is consistent with the simulation results.

The comparison results of the measured and simulated S_{21} are shown in Fig. 14. The test results are basically consistent with the simulation ones. Notably, the measured results indicate that the coupling coefficient S_{21} of the antennas with CSDGS is consistently lower than that of the antenna without CSDGS throughout the entire operating band (6.84 GHz–7.8 GHz).

Deviation between measurement and simulation results is not uncommon and can be attributed to various factors. In the specific case of the observed deviation between the measured and simulated results, potential reasons include the inherent lack of precision in antenna processing and the possibility of errors

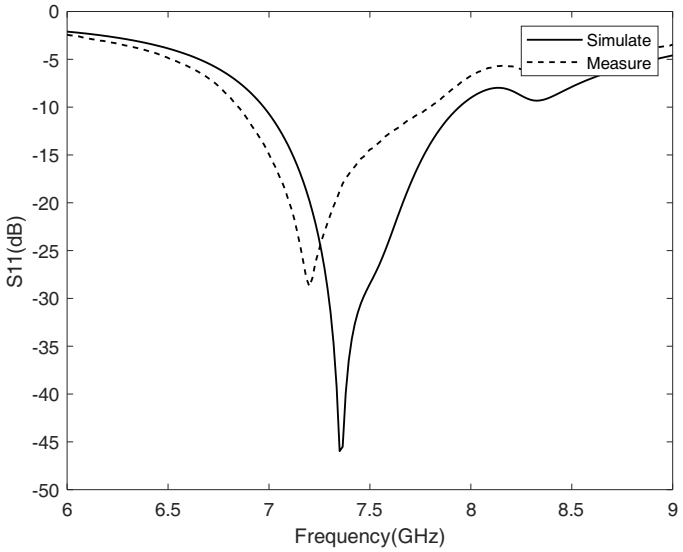

FIGURE 13. The results of simulation and measured S_{11}.

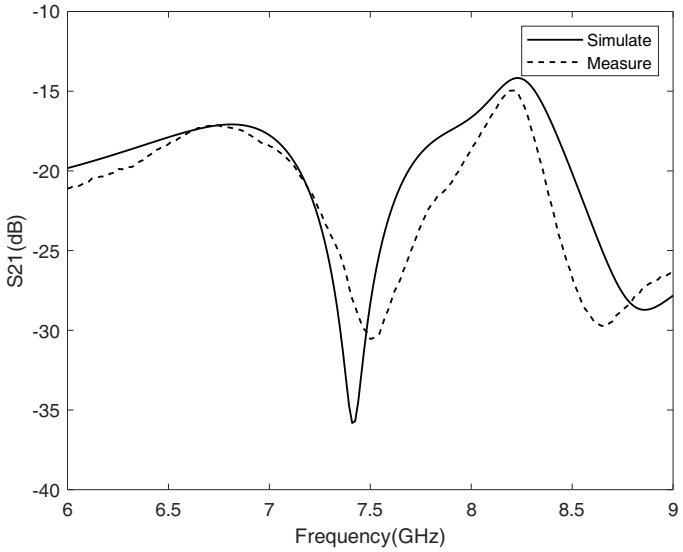

FIGURE 14. The results of simulation and measured S_{21}.

introduced during the instrument connections made during the measurement process.

4. CONCLUSION

The aim of this paper is to propose the CSDGS to reduce coupling between PIFAs. By etching the CSDGS into the ground plane of the PIFA, the coupling between its elements can be effectively suppressed. The addition of the CSDGS structure results in an increased operating bandwidth of the antenna by 0.25 GHz. Additionally, it leads to a reduction in the coupling between radiation elements by more than 22 dB at its maximum, with an average reduction of more than 11 dB within the 7.0 GHz–7.7 GHz range. These improvements greatly enhance the overall performance of the antenna. Both simulation and measurement results demonstrate that the incorporation of the CSDGS structure effectively suppresses the coupling between the elements of the antenna array. In conclusion, the CSDGS structure proves to be an effective solution for reducing coupling and enhancing the performance of PIFAs.

REFERENCES

[1] Fang, Y., Y. Liu, Y. Jia, J. Liang, and H. H. Zhang, "Reconfigurable structure reutilization low-SAR MIMO antenna for 4G/5G full-screen metal-frame smartphone operation," *IEEE Antennas and Wireless Propagation Letters*, Vol. 22, No. 5, 1219–1223, May 2023.

[2] Sheriff, N., S. K. A. Rahim, H. T. Chattha, and T. K. Geok, "Multiport single element mimo antenna systems: A review," *Sensors*, Vol. 23, No. 2, 747, Jan. 2023.

[3] Alibakhshikenari, M., F. Babaeian, B. S. Virdee, S. Aissa, L. Azpilicueta, C. H. See, A. A. Althuwayb, I. Huynen, R. A. Abd-Alhameed, F. Falcone, and E. Limiti, "A comprehensive survey on 'Various decoupling mechanisms with focus on metamaterial and metasurface principles applicable to SAR and MIMO antenna systems'," *IEEE Access*, Vol. 8, 192 965–193 004, 2020.

[4] Dey, S., S. Dey, and S. K. Koul, "Isolation improvement of MIMO antenna using novel EBG and hair-pin shaped DGS at 5G millimeter wave band," *IEEE Access*, Vol. 9, 162 820–162 834, 2021.

[5] Zhang, S. and G. F. Pedersen, "Mutual coupling reduction for UWB MIMO antennas with a wideband neutralization line," *IEEE Antennas and Wireless Propagation Letters*, Vol. 15, 166–169, 2015.

[6] Khandelwal, M. K., B. K. Kanaujia, and S. Kumar, "Defected ground structure: Fundamentals, analysis, and applications in modern wireless trends," *International Journal of Antennas and Propagation*, Vol. 2017, 2018527, 2017.

[7] Gao, D., Z.-X. Cao, S.-D. Fu, X. Quan, and P. Chen, "A novel slot-array defected ground structure for decoupling microstrip antenna array," *IEEE Transactions on Antennas and Propagation*, Vol. 68, No. 10, 7027–7038, Oct. 2020.

[8] OuYang, J., F. Yang, and Z. M. Wang, "Reducing mutual coupling of closely spaced microstrip MIMO antennas for WLAN application," *IEEE Antennas and Wireless Propagation Letters*, Vol. 10, 310–313, 2011.

[9] Chiu, C.-Y., C.-H. Cheng, R. D. Murch, and C. R. Rowell, "Reduction of mutual coupling between closely-packed antenna elements," *IEEE Transactions on Antennas and Propagation*, Vol. 55, No. 6, 1732–1738, Jun. 2007.

[10] Zhu, F. G., J. D. Xu, and Q. Xu, "Reduction of mutual coupling between closely-packed antenna elements using defected ground structure," *Electronics Letters*, Vol. 45, No. 12, 601–602, Jun. 2009.

[11] Huang, L., H. Zhao, Z. Hu, and Q. Cheng, "Reduction of mutual coupling between closely-packed antenna elements with split ring resonator (SRR)," in *2010 International Conference on Microwave and Millimeter Wave Technology*, 1873–1875, Chengdu, China, 2010.